

# Hysteretic behavior between quasi-two-dimensional flow and three-dimensional flow in forced rotating turbulence

Naoto Yokoyama\*

*Department of Aeronautics and Astronautics, Kyoto University, Kyoto 615-8540, Japan*

Masanori Takaoka†

*Department of Mechanical Engineering, Doshisha University, Kyotanabe 610-0394, Japan*

(Dated: September 19, 2018)

Conflict between formation of a cyclonic vortex and isotropization in forced homogeneous rotating turbulence is numerically investigated. It is well known that a large rotation rate of the system induces columnar vortices to result in quasi-two-dimensional (Q2D) flow, while a small rotation rate allows turbulence to be three-dimensional (3D). It is found that the transition from the Q2D turbulent flow to the 3D turbulent flow and the reverse transition occur at different values of the rotation rates. At the intermediate rotation rates, bistability of these two statistically steady states is observed. Such hysteretic behavior is also observed for the variation of the amplitude of an external force.

Formation of columnar structures parallel to a rotation axis is one of the most fundamental and distinctive phenomena in flows subject to rotation. The emergence of columnar vortices in the rotating turbulence makes a three-dimensional (3D) flow into a quasi-two-dimensional (Q2D) flow. The Taylor–Proudman theorem has succeeded in explaining the cylindrical flow in laboratory experiments and field observations in terms of the Taylor column. However, the theorem cannot describe transitions between the Q2D and 3D flows, because energy is exchanged between the Q2D mode and the 3D mode by nonlinear mechanisms [1]. The energy transfers to the Q2D modes were demonstrated by an instability analysis [2] and weak-turbulence theory in the large-rotation limit [3]. The Coriolis term breaks the parity invariance of the governing equation of the flow, and introduces a scale-independent time scale which induces two-dimensionalization at larger scales more effectively. Therefore, the Coriolis effect originates cyclone-anticyclone asymmetry with enhanced stretching of cyclonic vorticity and destabilization of anticyclonic one due to the centrifugal instability and the vortex tilting [4].

To classify the flow properties in rotating systems, the Rossby number  $Ro$ , which is the ratio between the linear and nonlinear time scales, has been used [5]. Note that though various definitions of  $Ro$  are used in literature, the following facts are independent of its detailed definition. When the Coriolis force is weak relative to turbulence, i.e.,  $Ro \gg 1$ , the 3D Kolmogorov turbulence is obtained. When  $Ro \sim 1$ , only cyclonic vortices appear at large scales, and the flow becomes Q2D. When  $Ro \ll 1$ , both cyclonic and anticyclonic vortices appear, and the flow fields are almost completely two-dimensionalized. The transitions between the Q2D turbulence and the 3D turbulence by changing the system’s rotation rate  $\Omega$  were numerically studied [6]. It was reported that  $Ro$ -dependence of turbulent statistics is not monotonic in the range  $Ro \sim 1$ , where the coherent vortices and inertial waves at small wave numbers and the turbulence at large wave numbers coexist [7, 8]. The two-dimensionalization and the cyclone-anticyclone asymmetry depend on the external forces and the boundary conditions (e.g., Ref. [9]).

Recently, Ref. [10] reported a phase diagram for statistically steady states of forced Taylor–Green flows in a rotating frame. Four different steady states in the parameter space spanned by the Reynolds numbers and the Rossby numbers were numerically obtained by carrying out 184 simulations. Subcritical behavior was implied by an abrupt transition between the Q2D and 3D flows. If it were a low-dimensional system, one might expect a hysteresis in such transition. Because the parameter space analysis was performed with the same random initial condition for every parameter values in Ref. [10], the hysteretic behavior cannot be directly found.

It has been experimentally found that there exists a parameter range where a high-torque state and a low-torque state are bistable and show a hysteretic behavior in a highly turbulent Taylor–Couette flow [11]. A similar hysteretic behavior was observed also in rotating spherical Couette flow [12]. Bistability and hysteresis between a stationary magnetic field and an oscillatory magnetic field in a low-dimensional phase space were observed in a turbulent flow of liquid sodium [13]. Note that the heteroclinic alternating transitions such as blocking in a rotating annulus [14] associated with the Lorenz attractor, where the state goes back and forth near the two *unstable* fixed points, are different from the bistability. Also note that the bistability does not necessarily indicate a hysteresis, which requires a form of subcritical properties. The dynamical systems theory developed in low-dimensional systems has successfully been applied to the onset of turbulence, e.g., unstable periodic orbits in wall turbulence [15]. The bifurcation structures embedded in developed turbulence would be a key to understand its nature.

\* yokoyama@kuaero.kyoto-u.ac.jp

† mtakaoka@mail.doshisha.ac.jp

Most of the hysteretic behavior in developed turbulence have been observed in the flows bounded by solid walls, and the boundary condition plays an important role in the hysteretic behavior. In this work, a hysteretic behavior in developed rotating turbulence are numerically investigated in a periodic box. As far as the authors are aware, such behavior in the system not bounded by the solid walls has rarely been reported. While the boundary condition and the forcing scheme in the present study are the same as those in Ref. [10], the analytical methodologies for the parameter dependence of the flow patterns are different; a flow field in the statistically steady state for a close parameter is employed as an initial condition in this study, whereas the random initial condition were used in Ref. [10]. The present approach is similar to the continuation of a solution which enables us to track a branch in multistability used in bifurcation analysis in low-dimensional dynamical systems.

We examine the dependence of flow properties on  $\Omega$  as well as the amplitude of the external force, focusing on the transition between the Q2D flow and the 3D flow. The micro-Rossby number defined below as well as the Taylor-scale Reynolds number is the first candidate to characterize the flow field. However, it is statistically defined by the flow itself, and cannot be used as a control parameter. The macro-Rossby number and the integral-scale Reynolds number can be control parameters, but they do not well characterize the turbulent field. As we will see below, the transitions are hysteretic owing to robustness of the large-scale columnar vortex against the turbulent fluctuation.

The governing equations for the velocity  $\mathbf{u}$  of the incompressible fluid are the Navier–Stokes equation with the Coriolis term and the divergence-free condition:

$$\frac{\partial \mathbf{u}}{\partial t} + (\mathbf{u} \cdot \nabla) \mathbf{u} + 2\boldsymbol{\Omega} \times \mathbf{u} = -\nabla p + \nu \nabla^2 \mathbf{u} + \mathbf{f}, \quad \nabla \cdot \mathbf{u} = 0,$$

where the centrifugal force is included in the pressure  $p$ . The rotation vector  $\boldsymbol{\Omega} = \Omega \mathbf{e}_z$  is assumed to be constant. The kinematic viscosity is expressed by  $\nu$ . Note that the small wave-number drag is not added, because it was reported that a statistically steady state can be achieved even for the inversely cascading two-dimensional turbulence [16]. The external force  $\mathbf{f}$  is given by the three-dimensional two-component force of a steady TG type  $\mathbf{f} = f_0 (\cos k_f x \sin k_f y \sin k_f z, -\sin k_f x \cos k_f y \sin k_f z, 0)$ , where  $k_f = 2$  is employed. The TG flow has also been used as a model of many laboratory flows (see Ref. [10]).

In the present simulations, the periodic boundary condition with the period  $(2\pi)^3$  is employed. The standard pseudo-spectral method with the aliasing removal by the phase shift and the spherical truncation is adopted for the nonlinear term, and the numerical resolution is  $512^3$ . The same value of  $\nu$  is used for all the series of the simulations. The Runge–Kutta–Gill method is adopted for the time integration, while the linear terms are calculated analytically. The characteristic length and time are selected so that the period of the computational box is  $2\pi$  and the Coriolis parameter  $2\Omega$  and the amplitude of the external force  $f_0$  are approximately 10.

Let us first consider  $\Omega$ -dependence. The rotation rate  $\Omega$  is set between 2.5 and 7.5 with 0.5 increments or decrements, while  $f_0$  is fixed at 10. The rotation rate is increased or decreased by 0.5 when the flow field for the previous rotation rate is in the statistically steady state. The Zeman wave numbers  $k_\Omega = (\Omega^3/\varepsilon)^{1/2}$ , where  $\varepsilon$  is the energy dissipation rate, are evaluated approximately as 1.4 for  $\Omega = 2.5$  and 16 for  $\Omega = 7.5$ . The corresponding flows are 3D and Q2D.

Since we are interested in the transitions between the Q2D turbulent flow and the 3D turbulent flow, the dependence of the  $zz$  component of the anisotropy tensor,  $b_{zz} = 1/3 - \langle u_z^2 \rangle / \langle |\mathbf{u}|^2 \rangle$ , on  $\Omega$  is drawn in Fig. 1 to evaluate the anisotropy of the flows. These values are obtained in the statistically steady states.

At  $\Omega = 2.5$ ,  $b_{zz} \approx 0.1$ , where the non-zero value comes from the anisotropic external force of the TG type. When the rotation rate is increased from  $\Omega = 2.5$  ( $\Omega \nearrow$ ),  $b_{zz}$  decreases to almost 0, where the flow is 3D and almost isotropic. It increases abruptly to about 0.3 in the range of  $5.5 < \Omega < 6$ , and the flow becomes Q2D and strongly anisotropic. At  $\Omega = 7.5$ ,  $b_{zz} \approx 0.3$  owing to the strong rotation. When the rotation rate is decreased from  $\Omega = 7.5$  ( $\Omega \searrow$ ),  $b_{zz}$  slowly decreases. In the range of  $4 < \Omega < 4.5$ ,  $b_{zz}$  drops sharply, representing the abrupt transition from the Q2D anisotropic flow to the 3D isotropic flow. In the range of  $4.5 \lesssim \Omega \lesssim 5.5$ , the two turbulent regimes are bistable and show a hysteretic behavior.

To characterize the upper- and lower-branch flows shown in Fig. 1, the Fourier- and the real-space properties at  $\Omega = 5$  are examined. The one-dimensional energy spectra are drawn in Fig. 2(a). For the lower-branch flow ( $\Omega \nearrow$ ), where  $k_\Omega \approx 8.6$ , the Kolmogorov spectrum  $k^{-5/3}$  appears all over the inertial subrange. For the upper-branch flow ( $\Omega \searrow$ ), while the Kolmogorov spectrum appears in the range  $k \gtrsim k_\Omega \approx 6.0$ , the energy spectrum at  $k \lesssim k_\Omega$  shows another turbulent state. A significant difference between the upper- and lower-branch flows appears at the small wave numbers; while the largest energy of the former appears at the scale of the external force,  $\sqrt{3}k_f \approx 3.46$ , that of the latter appears at the largest scale  $k = 1$ .

In the lower-branch flow, the energy supplied by the external force is almost completely transferred to the larger wave numbers as the 3D Kolmogorov turbulence. In the upper-branch flow, on the other hand, a part of the supplied energy is transferred to the smaller wave numbers owing to the quasi-two-dimensionalization, and the field reaches a statistically steady state when the accumulation at  $k \approx 1$ , more precisely  $(k_x, k_y, k_z) = (\pm 1, 0, 0), (0, \pm 1, 0)$ , is built up. The process of the accumulation is known as condensation. The inverse cascade due to the quasi-two-

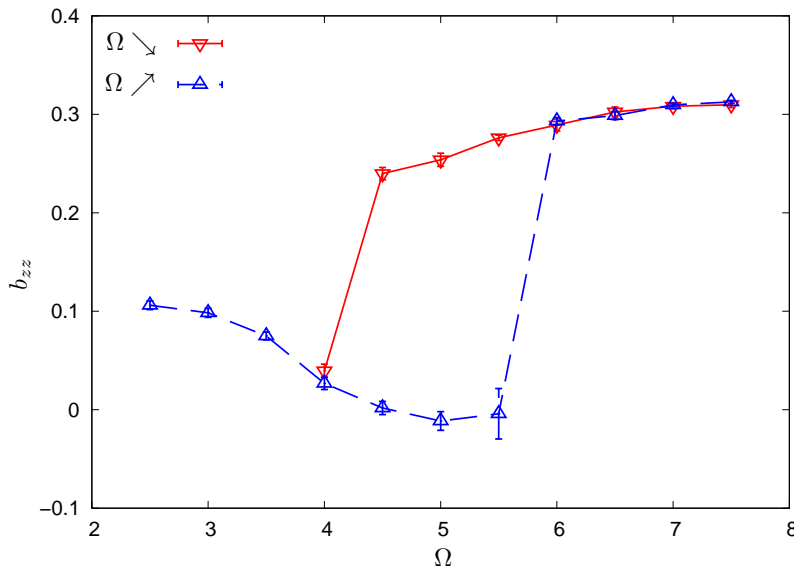


FIG. 1. Dependence of  $zz$  component of anisotropy tensor  $b_{zz}$  on  $\Omega$ . The solid curve ( $\Omega \searrow$ ) and the dashed curve ( $\Omega \nearrow$ ), respectively, show  $b_{zz}$  during the decrease of  $\Omega$  and the increase of  $\Omega$ . The error bars represent the standard deviation due to the time variation.

dimensionalization and the forward cascade from the accumulation to the large wave numbers are considered to balance with each other in the statistically steady state. Similar discussions can be found in Ref. [10].

The Q2D flow has larger energy than the 3D flow all over the wave numbers. Therefore, the two turbulent flows have different values of the micro-Rossby number  $Ro_{\omega_z} = \omega_{z\text{rms}}/(2\Omega)$  as well as the Taylor-scale Reynolds number  $Re_\lambda = (20E^2/(3\nu\varepsilon))^{1/2}$  under the identical parameters of the simulations:  $Ro_{\omega_z} \approx 2.5$  and  $Re_\lambda \approx 490$  in the Q2D flow, and  $Ro_{\omega_z} \approx 1.8$  and  $Re_\lambda \approx 110$  in the 3D flow. Here, the subscript rms denotes the root-mean square, and  $E$  is the total energy. Note that the Taylor microscale for the isotropic turbulence is used to obtain the values of  $Re_\lambda$ , because the Kolmogorov spectrum appears at the large wave numbers in both Q2D and 3D flows. The fact that  $Ro_{\omega_z}$  in the Q2D flow is larger than that in the 3D flow causes the non-monotonicity of the  $Ro$ -dependence of turbulent statistics as reported in Ref. [7].

Isosurfaces of vorticity norm  $|\boldsymbol{\omega}|$  in the real space are drawn in Figs. 2(b) and (c). In the lower-branch flow, Fig. 2(b), no large-scale vortex is formed, and we can observe only the small-scale 3D vortices. On the other hand, in the upper-branch flow, Fig. 2(c), the isosurfaces show the cyclonic vortex aligned along the rotation axis, which reminds us of the Taylor column. The cyclonic vortex makes strongly sheared regions between itself and its images due to the periodic boundary condition. In the strongly sheared regions, cylindrical swarm composed of anticyclonic small-scale vortices is produced, though they are weak. In fact, the cyclonic vortex makes a high-speed whirl as drawn on  $z = 0$  plane in Fig. 2(c), while the swarm does not. The cyclonic vortex accompanied by inertial waves makes the upper-branch flow Q2D.

Even though the simulations were run long, the possibility of transition between the Q2D flow and the 3D flow cannot be excluded. To confirm the bistability at  $\Omega = 5$ , the existence of a basin of attraction between the Q2D flow and the 3D flow is examined by starting from interpolated initial conditions. The initial conditions are made by the superposition of the Q2D flow and the 3D flow  $\mathbf{u} = r\mathbf{u}_{\text{Q2D}} + (1-r)\mathbf{u}_{\text{3D}}$ , where  $r \in [0, 1]$  is the weight for the interpolation between the Q2D flow and the 3D flow. The simulations are performed for the weights  $r = 0.1, 0.2, \dots, 0.9$  until each field reaches a statistically steady state.

The time evolutions of  $b_{zz}$ ,  $E$ , perpendicular energy  $E_\perp = \sum_{\mathbf{k}} |\tilde{\mathbf{u}}_\perp|^2/2$  and parallel energy  $E_\parallel = \sum_{\mathbf{k}} |\tilde{u}_z|^2/2$  for  $r = 0.2$  and  $0.3$  are drawn in Figs. 2(d) and (e). Here,  $\tilde{\mathbf{u}}_\perp$  is the Fourier coefficient of the velocity component perpendicular to the rotation axis  $\mathbf{u}_\perp = (u_x, u_y, 0)$ . In the simulation with  $r = 0.2$ ,  $b_{zz}$  decreases to around 0, while  $b_{zz}$  increases to around 0.25 in the simulation with  $r = 0.3$ . That is, the boundary separating the Q2D flow and the 3D flow exists in the range  $0.2 < r < 0.3$ , and the Q2D flow and the 3D flow are bistable at  $\Omega = 5$ . The separatrix might not be a thin boundary like the one which separates laminar and turbulent flows at the onset of turbulence [17] but a thick and blurred region.

It is of interest to note that both  $E_\parallel$ 's for  $r = 0.2$  and  $0.3$  remain small and the main difference appears in  $E_\perp$ . Since  $b_{zz} = 1/3 - E_\parallel/(E_\perp + E_\parallel)$ , the transitions between the Q2D flow and the 3D flow occur mainly in  $\mathbf{u}_\perp$ , i.e.,  $\omega_z$ .

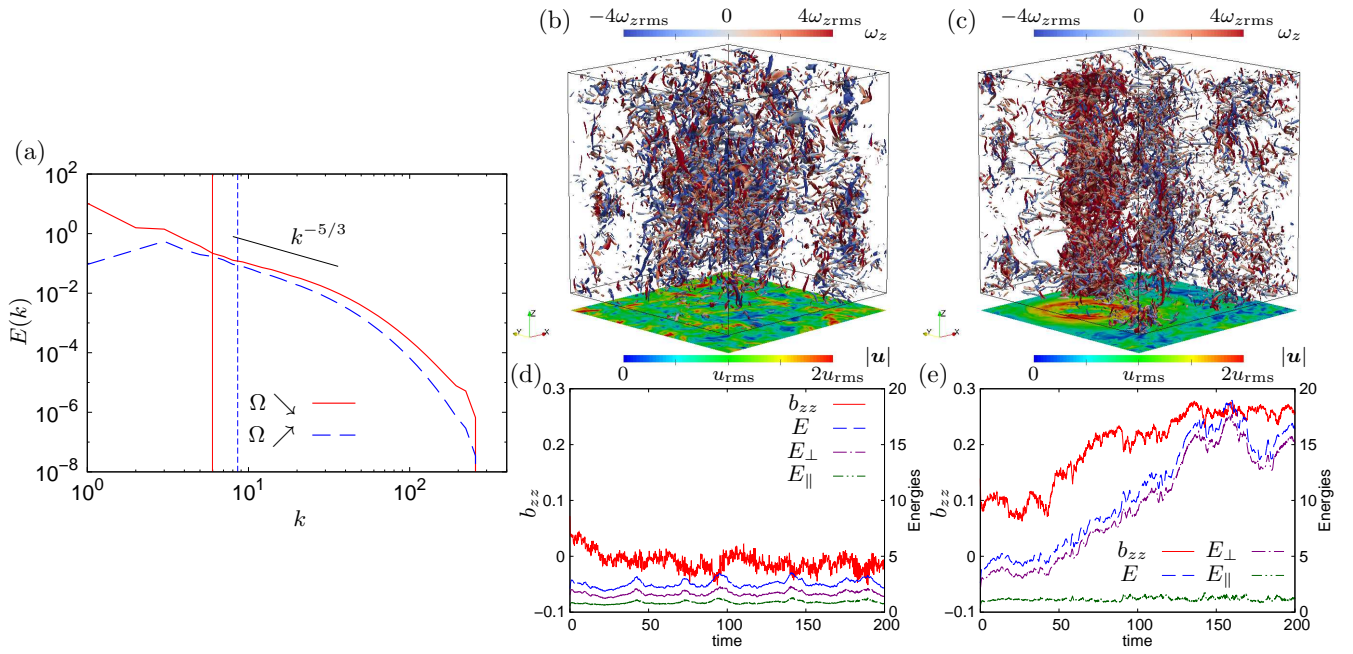


FIG. 2. Bistability between the Q2D flow and the 3D flow at  $\Omega = 5$ . Energy spectra (a). The vertical lines represent the Zeman wave numbers. Isosurfaces of  $|\boldsymbol{\omega}| = \pm 3\sqrt{\langle|\boldsymbol{\omega}|^2\rangle}$  colored by  $\omega_z$  and speed distribution on  $z = 0$  plane for lower branch  $\Omega \searrow$  (b) and for upper branch  $\Omega \nearrow$  (c). Time evolution of  $b_{zz}$  (left axis) and total, perpendicular and parallel energies (right axis) for the interpolation weight  $r = 0.2$  (d) and for  $r = 0.3$  (e) between the Q2D flow and the 3D flow.

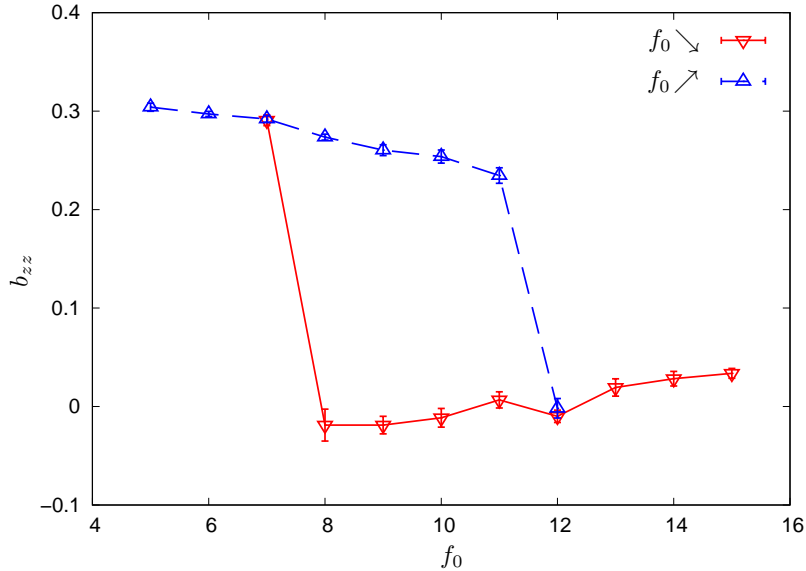


FIG. 3.  $f_0$ -dependence of  $b_{zz}$ . See also the caption of Fig. 1.

In other words, the fluctuation in the rotation direction,  $u_z$ , is little affected by the rotation.

At the transition from the 3D flow to the Q2D flow, the coherent cyclonic vortex is formed by overwhelming the external force as well as turbulent fluctuation. The external force in the present simulations tries to develop the TG vortices whose symmetries and scales are different from the coherent cyclonic vortex. On the other hand, at the reverse transition, the coherent vortex collapses into pieces. The formation and destruction of the large coherent vortex cannot be continuous for the variation of  $\Omega$ . Therefore, the transitions exhibit the hysteresis.

The dependence of  $b_{zz}$  on the amplitude of the external force  $f_0$ , which is increased with 1 increments or decreased

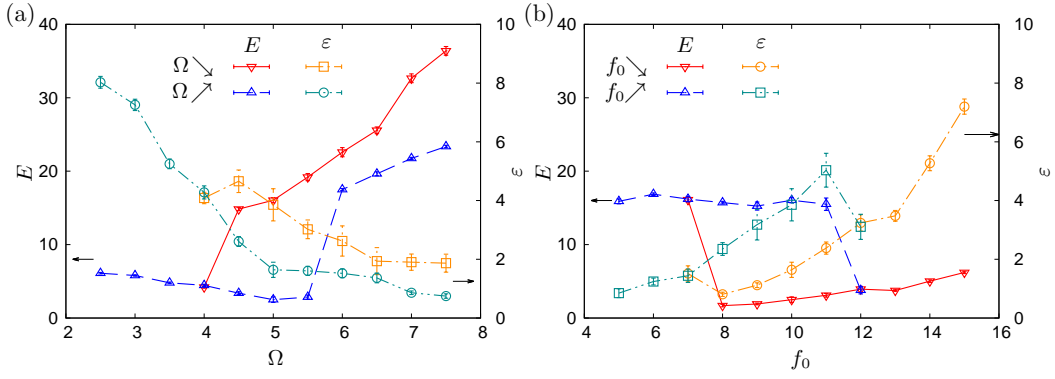


FIG. 4.  $\Omega$ -dependence (a) and  $f_0$ -dependence (b) of total energy (left axis) and energy dissipation rate (right axis).

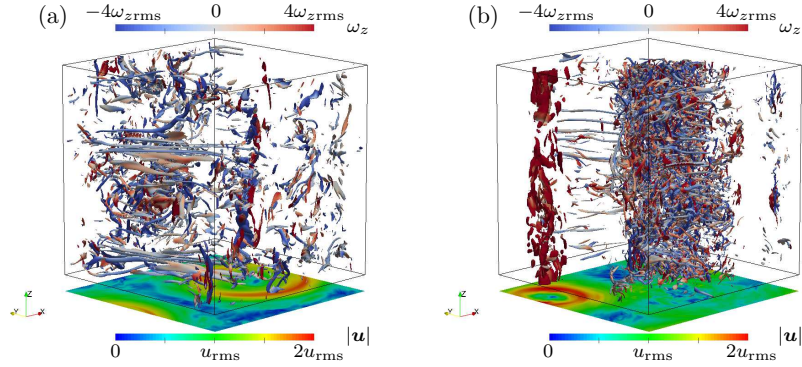


FIG. 5. Isosurface of  $|\omega| = \pm 3\sqrt{\langle |\omega|^2 \rangle}$  colored by  $\omega_z$  and speed distribution on  $z = 0$  plane at  $\Omega = 7.5$ . (a): lower branch, and (b): upper branch.

with 1 decrements, is drawn in Fig. 3. Following the results of the  $\Omega$ -dependence in Fig. 1, we here investigate the cases with  $\Omega = 5$  as representative. Similar to Fig. 1, the Q2D flow and the 3D flow are, respectively, observed at small  $f_0$  and large  $f_0$ , and the two turbulent flows are bistable and hysteretic at intermediate  $f_0$ . Obviously, this two-dimensionalization is due to the cyclonic vortex along the rotation axis.

To analyze the properties of the above hysteretic behaviors at the large and small scales, the dependences of the total energy  $E$  and the energy dissipation rate  $\varepsilon$  on  $\Omega$  and  $f_0$  are shown in Fig. 4. These figures show different behaviors between the  $\Omega$ - and  $f_0$ -dependences even qualitatively. The transitions of  $E$  and  $\varepsilon$  show the bistability in  $4.5 \lesssim \Omega \lesssim 5.5$  and  $8 \lesssim f_0 \lesssim 11$  as observed in Figs. 1 and 3. However, both  $E$  and  $\varepsilon$  have different values at large  $\Omega$  where the flow is Q2D. No clear jump in  $5.5 \leq \Omega \leq 6$  can be seen in  $\varepsilon$  for increasing  $\Omega$  in Fig. 4(a). In other words, small-scale dynamics is insensitive to  $\Omega$ , which is consistent with the fluctuation in the rotation direction,  $E_{\parallel}$ , observed in Figs. 2(d) and (e).

The fact that the discrepancy between the two branches at large  $\Omega$  is larger than the turbulent fluctuation and the hysteresis loop is not closed implies the multiplicity of the statistically steady states of the Q2D flows. The multiplicity is confirmed by finding the separatrix of the superposition of the two flows in the same way to demonstrate the bistability between the Q2D flow and the 3D flow at  $\Omega = 5$  (Figs. 2(d) and (e)). It should be noted that  $b_{zz}$  shown in Fig. 1, which is a non-dimensionalized quantity composed of the ratio of the parallel energy to the total one, is insensitive to the variation of the energies themselves.

It may appear to be counterintuitive that the total energy for the small external force is larger than that for the large external force as shown in Fig. 4(b). It can be explained by the formation process of the large-scale cyclonic vortex. When the external force is weak, the Coriolis force is strong relative to turbulence intensity. Then, the large-scale columnar vortex is formed, and it makes the large energy accumulation near  $k_z = 0$ . Conversely, when the external force is strong, the Coriolis force is relatively weak. Then, the turbulent flow is 3D, and all the energy supplied by the external force is cascaded forwardly. As a result, the energy does not accumulate near  $k_z = 0$ , and the total energy is small.

Lastly, to investigate the characteristics of the multiplicity at the large  $\Omega$ , the isosurfaces of  $|\omega|$  for each branch

at  $\Omega = 7.5$  are shown in Fig. 5(a). Obviously, both flows have the Q2D structures as indicated in Fig. 1. While the upper-branch flow has the strong slender cyclonic vortex accompanied by the swarm of anticyclonic small vortices, the cyclonic vortex in the lower-branch flow is weak and fat, and there is no room for the anticyclonic swarm to grow. These flow patterns as well as the total energy and the energy dissipation rate reveal the distinctive features degenerated in the representation in terms of  $b_{zz}$ . The Q2D flow might have more multiplicities other than those shown here.

Comparing with the phase diagram in Ref. [10], we recognize that most of the parameter values in the present study fall into the quasi-2D condensates, while some are located narrowly in the range of intermittent bursts and weakly rotating flows. The quasi-2D condensates and the weakly rotating flows in Ref. [10] respectively correspond to the Q2D flow and the 3D flow reported here. An abrupt change in energy due to variation of Rossby number between the Q2D flow and the 3D flow was observed, and the subcritical behavior was implied by the abrupt change. It should, however, be noted that the initial conditions used in Ref. [10] were not the solutions for other parameters. In this Rapid Communication, the Q2D and 3D branches were traced by continuing the solution to find whether the subcritical behavior results in the hysteretic behavior or the heteroclinic alternating transitions in large turbulent fluctuations. The intermittent bursts are not observed in this study, but intermittent growths of the total energy which are caused by the energy transfers to the small wave numbers for a short time appear in the 3D flow as recognized in Fig. 2(d). The intermittent growths in the 3D flow are more frequent and not so strong than the intermittent bursts observed in Ref. [10].

In summary, the  $\Omega$ -dependence and the  $f_0$ -dependence of turbulent flows were investigated by numerically simulating the Navier–Stokes equation with the Coriolis term under the steady forcing of the TG type. The hysteretic behavior between the Q2D flows observed at large  $\Omega$ 's and the 3D flows at small  $\Omega$ 's was found. This hysteretic behavior stems from the robustness of the large-scale cyclonic columnar vortex. The hysteretic behavior between the Q2D flow and the 3D flow exists for a finite bounded area in  $(\Omega, f_0)$ . Although the flow properties had been classified simply by using the micro-Rossby number [7] and summarized in a phase diagram in Ref. [10], the present results demonstrate that the selection of the flow structures depends also on the initial conditions. The hysteresis brings the complexity of Ro-dependence at  $\text{Ro} \sim 1$ .

This hysteretic behavior robustly exists against the large fluctuation of the fully developed turbulence whose energy spectra show the  $-5/3$  power law. We also performed preliminary simulations in which flows are excited by a white random force [18]. The hysteresis and the bistability between the Q2D turbulent flow and the 3D turbulent flow are observed also for such antithetical forcing, though the range of the bistable parameters is much smaller. The existence of the universal mechanism for the emergence of multiple flow patterns in turbulence is expected. Dependence of the hysteretic behavior on the forcing types, the multiplicity of the Q2D flow, and the formation mechanism of the hysteretic behavior will be reported elsewhere.

## ACKNOWLEDGMENTS

Numerical computation in this work was carried out at the Yukawa Institute Computer Facility, Kyoto University and Research Institute for Information Technology, Kyushu University. This work was partially supported by JSPS KAKENHI Grant No. 15K17971 and No. 16K05490.

- 
- [1] F. Bellet, F. S. Godeferd, J. F. Scott, and C. Cambon, “Wave turbulence in rapidly rotating flows,” *J. Fluid Mech.* **562**, 83–121 (2006).
  - [2] F. Waleffe, “The nature of triad interactions in homogeneous turbulence,” *Phys. Fluids A* **4**, 350–363 (1992); “Inertial transfers in the helical decomposition,” **5**, 677–685 (1993); L. M. Smith and F. Waleffe, “Transfer of energy to two-dimensional large scales in forced, rotating three-dimensional turbulence,” **11**, 1608–1622 (1999).
  - [3] S. Galtier, “Weak inertial-wave turbulence theory,” *Phys. Rev. E* **68**, 015301 (2003).
  - [4] P. Bartello, O. Métais, and M. Lesieur, “Coherent structures in rotating three-dimensional turbulence,” *J. Fluid Mech.* **273**, 1–29 (1994); C. Cambon, J.-P. Benoit, L. Shao, and L. Jacquin, “Stability analysis and large-eddy simulation of rotating turbulence with organized eddies,” **278**, 175–200 (1994); B. Sreenivasan and P. A. Davidson, “On the formation of cyclones and anticyclones in a rotating fluid,” *Phys. Fluids* **20**, 085104 (2008).
  - [5] E. J. Hopfinger, F. K. Browand, and Y. Gagne, “Turbulence and waves in a rotating tank,” *J. Fluid Mech.* **125**, 505–534 (1982); J. Bardina, J. H. Ferziger, and R. S. Rogallo, “Effect of rotation of isotropic turbulence: computation and modeling,” **273**, 1–29 (1985); P. K. Yeung and Y. Zhou, “Numerical study of rotating turbulence with external forcing,” *Phys. Fluids* **10**, 2895–2909 (1998).
  - [6] L. M. Smith, J. R. Chasnov, and F. Waleffe, “Crossover from two- to three-dimensional turbulence,” *Phys. Rev. Lett.*

- 77**, 2467–2470 (1996); E. Deusebio, G. Boffetta, E. Lindborg, and S. Musacchio, “Dimensional transition in rotating turbulence,” *Phys. Rev. E* **90**, 023005 (2014).
- [7] L. Bourouiba and P. Bartello, “The intermediate Rossby number range and two-dimensional–three-dimensional transfers in rotating decaying homogeneous turbulence,” *J. Fluid Mech.* **587**, 139–161 (2007).
- [8] A. Campagne, B. Gallet, F. Moisy, and P.-P. Cortet, “Disentangling inertial waves from eddy turbulence in a forced rotating-turbulence experiment,” *Phys. Rev. E* **91**, 043016 (2015).
- [9] F. S. Godeferd and F. Moisy, “Structure and dynamics of rotating turbulence: A review of recent experimental and numerical results,” *Appl. Mech. Rev.* **67**, 030802 (2015).
- [10] A. Alexakis, “Rotating Taylor–Green flow,” *J. Fluid Mech.* **769**, 46–78 (2015).
- [11] S.G. Huisman, R.C.A. van der Veen, C. Sun, and D. Lohse, “Multiple states in highly turbulent Taylor–Couette flow,” *Nat. Commun.* **5**, 3820 (2014); S. Grossmann, D. Lohse, and C. Sun, “High-Reynolds number Taylor–Couette turbulence,” *Annu. Rev. Fluid Mech.* **48**, 53–80 (2016); R. C. A. van der Veen, S. G. Huisman, O.-Y. Dung, H. L. Tang, C. Sun, and D. Lohse, “Exploring the phase space of multiple states in highly turbulent Taylor–Couette flow,” *Phys. Rev. Fluids* **1**, 024401 (2016).
- [12] D. S. Zimmerman, S. A. Triana, and D. P. Lathrop, “Bi-stability in turbulent, rotating spherical Couette flow,” *Phys. Fluids* **23**, 065104 (2011).
- [13] M. Berhanu, B. Gallet, R. Monchaux, M. Bourgoïn, PH. Odier, J.-F. Pinton, N. Plihon, R. Volk, S. Fauve, N. Mordant, F. Pétrélis, S. Aumaitre, A. Chiffaudel, F. Daviaud, B. Dubrulle, and F. Ravelet, “Bistability between a stationary and an oscillatory dynamo in a turbulent flow of liquid sodium,” *J. Fluid Mech.* **641**, 217–226 (2009).
- [14] E. R. Weeks, Y. Tian, J. S. Urbach, K. Ide, H. L. Swinney, and M. Ghil, “Transitions between blocked and zonal flows in a rotating annulus with topography,” *Science* **278**, 1598–1601 (1997).
- [15] G. Kawahara and S. Kida, “Periodic motion embedded in plane Couette turbulence: regeneration cycle and burst,” *J. Fluid Mech.* **449**, 291–300 (2001).
- [16] C.-K. Chan, D. Mitra, and A. Brandenburg, “Dynamics of saturated energy condensation in two-dimensional turbulence,” *Phys. Rev. E* **85**, 036315 (2012).
- [17] T. Itano and S. Toh, “The dynamics of bursting process in wall turbulence,” *J. Phys. Soc. Jpn.* **70**, 703–716 (2001); T. M. Schneider and B. Eckhardt, “Edge states intermediate between laminar and turbulent dynamics in pipe flow,” *Phil. Trans. R. Soc. A* **367**, 577–587 (2009).
- [18] See Supplemental Material at [URL will be inserted by publisher] for hysteresis and bistability in rotating turbulence excited by a random white force.